Improved strength and control over surface-magnetized titania porous structures freeze cast under oscillating magnetic fields

Josh R. Fernquist [*], Isaac Nelson, Ashkan Pourkand, Jake J. Abbott, Steven E. Naleway

University of Utah, Department of Mechanical Engineering, Salt Lake City, UT, United States

ARTICLE INFO

ABSTRACT

Fabrication processes that produce porous structures with a high strength-to-weight ratio are sought after in many industries. The process of freeze casting is a way to achieve these porous structures with high strength-to-weight ratios, but only in a single direction (the direction of the templating-ice growth). Application of a magnetic field to these structures allows for an increase of mechanical strength in an additional orthogonal direction, therefore allowing them to be applied in more complex loading scenarios. Using a Helmholtz coils setup, it is possible to apply weak, uniform fields (<10 mT) in a variety of directions, magnitudes, or frequencies. Previous research has shown that the application of these weak uniform fields, in particular, oscillating fields from a Helmholtz coils setup, has led to increased mechanical strength through microstructural alignment, but only when using iron oxide structures. To mitigate this, a surface magnetization process was used to increase the magnetic response from non-ferrimagnetic materials, specifically titania, along with a higher magnetic strength (20 mT) Helmholtz coils setup. These surface-magnetized materials and oscillating fields led to an increase of strength of 10x when compared to non-surface-magnetized materials and 2x when compared to surface-magnetized materials under no field due to decreased porosity and increased alignment of mineral bridges. This demonstrates that increased material response for non-ferrimagnetic titania can be induced through the application of an oscillating field in conjunction with the surface-magnetization process.

1. Introduction

The freeze-casting process is a fabrication technique that has been extensively researched over the past 20 years [1,2]. This is due to the ease in fabricating each type of engineering material; polymers [3–7], metals [8–11], composites [12,13], and ceramics [14–17]. The typical freeze-casting process consists of:

1. Mixing a slurry that consists of a freezing agent, one or multiple solid loading compounds, binder(s), and additional additives such as dispersants.
2. Directionally freezing the mixed slurry, usually by pouring the slurry into a mold attached to a cold finger submerged in a cold bath. This causes the freezing agent to directionally solidify and template the structure.
3. Placing the solidified body in a freeze dryer to sublimate the ice crystals, resulting in a porous green body, or a fragile porous structure held together only by a polymeric binder.
4. Densifying said green body (e.g., by sintering in a furnace). This allows the green body to form a dense porous structure, templated by the grown ice crystals.

Aside from differing solid loading compounds that have been used in freeze casting (e.g., titania [9], iron oxide [18], alumina [19], zirconia [20]), many different intrinsic and extrinsic factors have been studied in the freeze-cast fabrication process to achieve material response. An intrinsic factor is one that is changed internally, such as varying the freezing rates [21–23] or the use of additional slurry additives [19,20,24–26]. An extrinsic factor is one that is applied externally, such as changing the freezing direction [27–33] or application of external forces (e.g., electric, acoustic, magnetic) [17,19,33,34]. The application of magnetic fields to freeze-cast structures in particular has recently been shown to induce significant increases in mechanical properties through the alignment of the microstructure [17–19,34–36].

These externally applied magnetic fields have been of particular interest due to the basic freeze-casting process producing structures that are mechanically strong in the ice-growth direction but weak in the two

---

* Corresponding author.
E-mail address: josh.fernquist@utah.edu (J.R. Fernquist).

orthogonal directions [19,35]. By applying these magnetic fields transverse to the ice growth direction, it has been shown to lead to increases of mechanical strength in this transverse direction, with increases of up to 3x in compressive strength [18,34].. To achieve these results, the magnetic field was applied during the freezing process (step 2 above), as this is when the particles, which are suspended in the freezing agent, are the most susceptible to the magnetic field [34,36,37]. Many of these studies utilized setups with permanent magnets to apply fields during the freeze-casting process [19,35,38,39]. While these setups allow for fields of large magnitudes to be produced (e.g., > 100 mT), this is done at the cost of creating a large magnetic-field gradient [38]. This gradient is caused due to the field strength near the permanent magnets being significantly greater than the field strength at the center of the setup [38]. The field gradient will lead to the migration of the magnetic particles to the surfaces closest to the magnetic of the freeze-cast structure, thus causing particle agglomeration [39]. This plating leads to an inhomogeneity of the material density and strength.

To combat this loss of bulk strength, recent research has shown the capability to impact freeze casting through the application of magnetic fields with little to no gradient [18,34,36]. This field uniformity allowed for the alignment of the particles without particle migration and agglomeration toward the surface (i.e., plating), which creates structures that are stronger in an orthogonal direction in addition to the ice-growth direction. In order to achieve these uniform fields, a Helmholtz coils setup was used [34]. Helmholtz coils are a pair of symmetric electromagnets that are spaced such that the distance between them is equal to the radius of each coil and can therefore apply nearly uniform fields in the free space between them [34,40]. To apply multiple fields simultaneously, pairs of coils can be arranged orthogonally to one another while still maintaining their field uniformity. A common configuration of multiple coils is the bi-axial Helmholtz coils, which are two sets of coils arranged orthogonally from one another. This configuration allows the user to apply a magnetic field in multiple directions simultaneously. This bi-axial setup has allowed users to apply complex fields during the freeze-casting process, such as diagonal [34], rotating [41], and oscillating fields [36], all of which allowed for complex control over the freeze-casting process. In these cases, all structures have been fabricated using iron oxide, a ferrimagnetic material, as this material is susceptible to the low magnitude fields generated [34,36]. While it is beneficial to achieve control over iron oxide scaffolds, greater benefit could be gained from achieving a similar level of control over non-ferrimagnetic materials, e.g. diamagnetic titania, as these materials tend to be more biocompatible and can be utilized to widen the range of applications (e.g., microplastic filters and bone implants [42]). The process of surface magnetization could aid in increasing the material response from non-ferrimagnetic materials [35,34]. While alignment and control has been achieved in other structures, such as nanotubes [43] and microspheres [44], significant improvements have yet to be seen for freeze-cast materials.

In addition to the surface-magnetization process, the application of oscillating fields during the freeze-casting process could increase material response from non-ferrimagnetic materials. An oscillating field consists of two differing field types applied simultaneously but in differing orthogonal directions [36]. The first is a constant field of a stronger magnitude in a single direction while the second is a weaker alternating field in an orthogonal direction from the first [36]. Application of these oscillating fields during the freeze-casting process has led to increased material response of freeze-cast ferrimagnetic materials, with a 2.5x increase in mechanical strength when compared to structures freeze cast under constant fields, through the alignment of the microstructure [36]. To this end, this research will focus on applying oscillating fields during the freeze-casting process to surface-magnetized non-ferrimagnetic titania, to achieve similar increases in material response as those from ferrimagnetic materials. The combination of oscillating magnetic fields and the surface magnetization process were demonstrated to provide enhanced non-ferrimagnetic titania material response when combined with freeze casting.

2. Materials and methods

2.1. Generation of constant magnetic field

Similar to previous studies, the magnetic fields applied in this study have a negligible gradient, i.e., at any given instant the field is effectively the same magnitude across all points of the workspace [18,36]. A bi-axial Helmholtz coils setup was fabricated and utilized to produce these uniform fields (Fig. 1). The Helmholtz coils setup was designed and fabricated based on previous design and fabrication procedures [34, 40], but with a few notable differences. A thermocouple was placed inside each coil to monitor the temperature while in operation. The temperature was monitored via a computer using the Arduino software. In addition, the coils were powered via an Advanced Motion Controls power supply and amplifier (Calle Tecate, Camarillo, CA) which are able to achieve 50 Amps, which is 1.5x stronger than previous setups used for magnetic freeze casting [36]. With the combination of temperature monitoring and the stronger amplifiers, these coils were capable of producing fields >20 mT without harm to the coils or the user. However, these larger fields led to a larger increase in the inductance of the coils and therefore a potentially slower system response time from the bi-axial setup, but this was compensated by the chosen power supply which was capable of generating large overhead voltage to increase the system response time and be capable of producing higher frequency fields, similar to previous setups [18,34,36]. Once fabricated, the setup was controlled through a computer utilizing LabVIEW software, which allowed the user to specify the magnitude, direction, and frequency of the applied field in one or multiple directions, those being the x- and y-directions. The y-direction corresponds with the vertical or ice-growth direction and the x-direction corresponds with the direction of the constant applied field (Fig. 1). Similar procedures to previous studies were used to verify the uniformity of the fields produced by this setup [34]. Magnetic field measurements of the workspace were taken using a 3-axis Hall magnetometer with $a \pm 1$ % accuracy (Metrolab THM1176, Geneva, Switzerland). Measurement locations were determined based on previous research to well-classify the magnetic field throughout the workspace [34]. A visual of the locations where measurements were taken can be seen in Fig. 2. The percent error of each measured location was then calculated using the formula:

$$\% \text{ error} = \frac{\| \overrightarrow{b}_i - \overrightarrow{b}_A \|}{\| \overrightarrow{b}_A \|} \cdot 100 \qquad (1)$$

where $\overrightarrow{b}_A$ is the magnetic field vector in the center of the center of the workspace (which corresponds to the center of the freeze-cast slurry), or position A as seen in Fig. 2, and $\overrightarrow{b}_i$ is the magnetic field vector at any position in the workspace (e.g., B, C, or D). This calculation was repeated for both sets of coils.

2.2. Surface magnetization

For this experiment, titania (TiO$_2$), from ACROS Organics (Pittsburgh, PA, USA) was first surfaced magnetized using established procedures [13,16,18]. 40 g of the microparticle (~10 μm) was added to 132 mL of water and, separately, 10 mL of anionic ferrofluid from Amazing Magnets (Anaheim, CA, USA) containing 3.9 vol% superparamagnetic iron oxide nanoparticles (SPIONs (~10 nm)) were added to 65.6 mL of water. The ferrofluid mixture was then added in increments of 10 mL to the titania mixture and stirred for one minute. The titania-ferrofluid mixture was then ball rolled for 24 h, vacuum filtrated and rinsed three times with water to remove any surfactant, then dried in for 24 h at 100 °C. Images using a transmission electron microscope (JEM 1400 TEM (120 keV), Salt Lake City, UT) and energy-dispersive
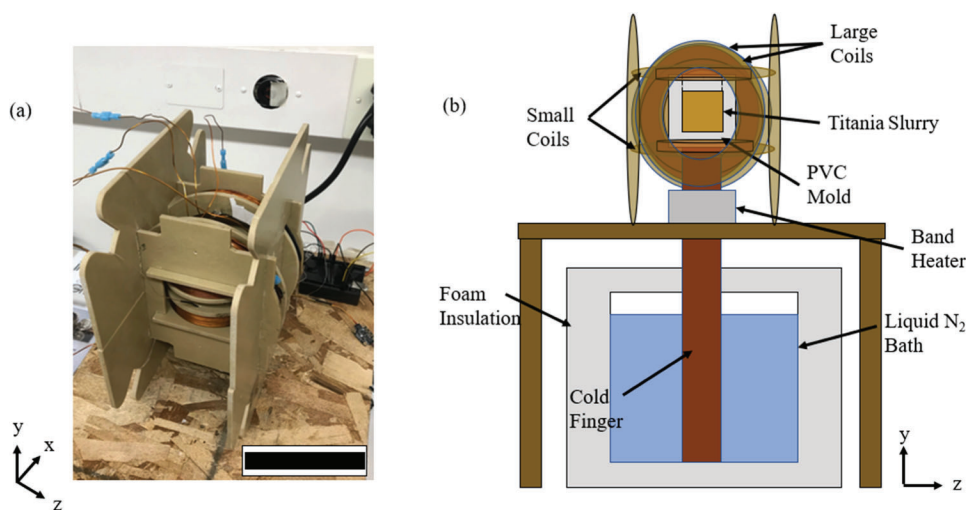
Fig. 1. (a) Trimetric view of the bi-axial Helmholtz coils used in the research along with coordinate system used herein. The large coils with the x-direction or applied field direction, and the small coils with the y-direction or ice-growth direction. (b) Detailed diagram of the freeze casting setup. The Helmholtz coils are placed over the PVC mold and slurry during the freezing process. The scale bar corresponds to 10 cm. (For interpretation of the references to color in this figure legend, the reader is referred to the web version of this article.).
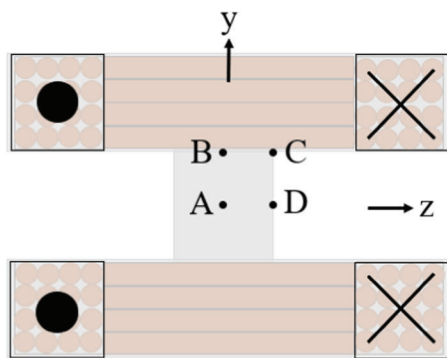

Fig. 2. Illustration of the locations where the field magnitude of the Helmholtz coils was measured, those being A (center), B (top center), C (top right), and D (right center). (For interpretation of the references to color in this figure legend, the reader is referred to the web version of this article.).

x-ray spectroscopy (EDS) were used to observe how the SPIONs interacted with the titania microparticles. Magnetic moments were measured using a vibrating sample magnetometer (EZ-7 VSM, Salt Lake City, UT) to provide mass magnetization (emu/g).

2.3. Sample preparation

Once surface magnetized, either surface-magnetized titania or non-surface-magnetized titania particles were used in all slurries as the solid loading compound. The slurry consisted of titania with a nominally spherical particle shape ($\leq 10\,\mu m$, Sigma Aldrich, St. Louis, MO) at 10 wt % with H_2O being used as the freezing agent in addition to binders polyvinyl alcohol (PVA) at 1 wt% and polyethelyne glycol (PEG) at 1 wt %, additive octanol at 0.435 wt% as an anti-foaming agent, and the dispersant Darvan 811 at 1 wt%. Each slurry was 11 mL in total volume. Each slurry was mixed on a vortex mixer for 2 min and then degassed under vacuum for 5 min. Once degassed the slurries were immediately poured into a PVC mold atop a cold finger sitting in a bath of liquid N_2 in a custom freeze-casting setup, as previously described [36]. A thermocouple and band heater were attached to the cold finger to monitor the temperature and to decrease it at a constant rate of 10 °C per min. All slurries were directionally frozen in the y-direction. A total of 20 scaffolds were fabricated from the following field types:

- No Field: no field applied during the freeze-casting process

- Constant Field: field was applied in the x-direction at constant magnitude of 20 mT
- 30 % Oscillation: field was applied in x-direction at a constant magnitude of 20 mT, along with an alternating field in the y-direction ranging between 6 mT and −6 mT at 5 rpm.

Five each being fabricated under the field types No Field and Constant Field, and 10 fabricated under the 30 % Oscillation. Surface-magnetized titania was used for all the No Field and Constant Field scaffolds, while half of the 30 % Oscillation scaffolds were fabricated with surface-magnetized titania, and the other half with non-surface-magnetized titania. Non-surface-magnetized scaffolds were fabricated under 30 % Oscillation in order to compare how the surface magnetization process affects the microstructure in addition to the application of oscillating fields. In addition, due to preliminary experiments, it was determined that simple field types had no effect on non-surface-magnetized titania, and therefore the ideal, or oscillating field type [36], was applied to non-surface-magnetized titania to see if any level of control was possible. In all cases, the fields were applied throughout the entire freezing process. After freezing the slurries, they were all lyophilized at 0.047 mBar and −61 °C in a Labconco Free Zone 1 freeze drier (Kansas City, MO, USA) for 72 h to sublimate all the ice crystals from the scaffolds. Once lyophilized, the green bodies were placed in an open-air Keith KSK-12 1700 furnace (Pico Rivera, CA, USA) and sintered at 1200 °C for 2 h, with a heating and cooling rate of 3 °C per min, resulting in solid scaffolds that could then be mechanical tested and analyzed.

2.4. Mechanical testing

Each scaffold was mechanically tested on an Instron 5967 load frame with an Instron 30 kN load cell (Norwood, MA, USA). The scaffolds were prepared for mechanical testing by cutting eight cubes from the midsection of each scaffold (see Fig. 3). From each scaffold, four of the cubes were compressed normal to the y-direction or ice-growth direction, and four cubes were compressed normal to the x-direction, or the direction of the applied constant magnetic field. Each cube had an average height of 5 mm and an average area of 25 mm^2. Each cube was compressed at a crosshead speed of 1 mm min^{-1}. The ultimate compression strength (UCS) and modulus of elasticity (E) were recorded during each test with the UCS being recorded as the highest engineering compression stress and the E being recorded as the slope of the linear-elastic region of the stress-strain curve. A total of 20 compression tests were completed in each of the x-direction and y-direction for No Field, Constant Field, 30 % Oscillation for the surface-magnetized scaffolds, and 30 % Oscillation for non-surface-magnetized scaffolds. The four
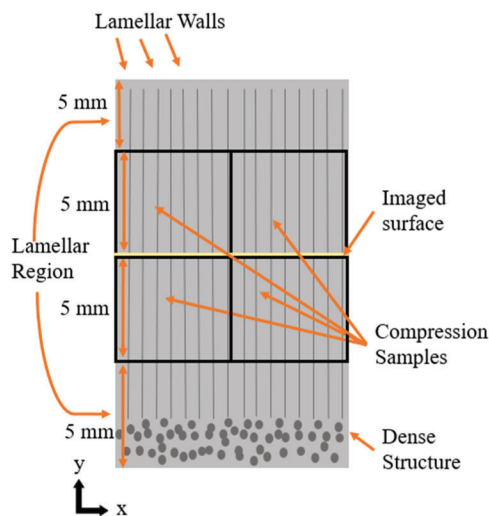
Fig. 3. An illustrated, cross-sectional diagram of a scaffolds and what samples were used. The bottom ~5 mm of the scaffold are removed due to the formation of dense structures. The compression samples begin ~5 mm from the bottom of the scaffold and are ~5 mm in height. The top surface of the bottom sample was used for SEM analysis (imaged surface), then all cubes were mechanically tested, with half being tested normal to the x-direction and half normal to the y-direction. (For interpretation of the references to color in this figure legend, the reader is referred to the web version of this article.).

repeated measures of a given quantity were averaged to estimate the value for that scaffold.

2.5. Material characterization

To view and characterize the microstructures of the scaffolds, images were taken of scaffolds for each field type using a scanning electron microscope (SEM, FEI Quanta 600 FG, Hillsboro, Oregon, USA). For each scaffold, the top face of the bottom cube cut from each scaffold was imaged (see Fig. 3) so as to image material from the center of the scaffold. All images were taken on the x-z face. A total of 20 scaffolds were imaged, with five each for No Field, Constant Field, 30 % Oscillation with surface-magnetized scaffolds, and 30 % Oscillation with non-surface-magnetized scaffolds. These images were analyzed using Image J software. This software allowed for the measurement of wall thickness, area porosity, pore area, pore major axis length, and pore minor axis length. All measurements were made on 500x magnification images. The results of these were the mean of 400 measurements from five scaffolds for each of the No Field, Constant Field, 30 % Oscillation with surface-magnetized scaffolds, and 30 % Oscillation with non-surface-magnetized scaffolds for the wall thickness, as well as the mean of 4400 measurements from five scaffolds for the area porosity, average pore size, and length of the major and minor axis. The wall thickness, major axis, and minor axis were all recorded in units of micrometers (μm), the average pore size was recorded in units of micrometers squared (μm^2), and the area porosity was recorded in a unitless percentage (%).

The lamellar wall alignment was analyzed using ImageJ software to further quantify how the microstructure changed as a function of the field type. The images were analyzed along the x-z face. Using a previously published process [18,36], walls were measured and binned into six separate sectors ($-60° \pm 15°$, $-30° \pm 15°$, $0° \pm 15°$, $30° \pm 15°$, $60° \pm 15°$ and $90° \pm 15°$) to determine the relative directionality of the walls.

Further alignment analysis was done by analyzing the alignment of the SPION-titania particles of the microstructures using an energy-dispersive detector (FEI Quanta 600 FE-ESEM w/ EDS, Salt Lake City, UT). The EDS was able to map out the location of the SPION-titania

microparticles in the microstructure, where the SPION-titania particles formed into rough walls, and then the direction of said walls were analyzed using ImageJ software. What constituted a "wall" versus an "agglomeration of particles" was defined as a string of continuous particles at least 50 μm in length (see Fig. 4). Similar to the analysis of the lamellar-wall directionality, the SPION-titania walls were measured and binned into six separate sectors ($-60° \pm 15°$, $-30° \pm 15°$, $0° \pm 15°$, $30° \pm 15°$, $60° \pm 15°$ and $90° \pm 15°$) to determine the relative directionality of the walls. The $0°$ sector corresponds to the direction of the applied magnetic field (x-direction). If the wall was measured to be in said sector, it was noted as such. The total number of walls in each sector was then divided by the total number of walls measured, leading to the percent walls in each sector.

2.6. Statistical analysis

A statistical analysis was run on the mechanical and image data of the scaffolds using a one-way ANOVA test in MATLAB software. The three different field types were considered, those being No Field, Constant Field, 30 % Oscillation with surface-magnetized particles, or 30 % Oscillation with non-surface-magnetized particles. Each test was run using a standard significant of $\alpha = 0.05$; if the test returned with a p-value less than the α value, then there were statistically significant differences in the tested data. If statistical significance was identified, a Tukey's Honest Significant Difference (HSD) test was then run on the data to view the significance of individual pair-wise comparisons.

A chi-square goodness to fit test was run on the alignment of the microstructure as well. This test was chosen because, when no magnetic field is applied, it would be expected to observe an approximately even distribution of the microstructure wall alignment across all sectors, with any differences due to random effects [18,36]. If one sector has a significantly higher number of walls than the others it would suggest an uneven distribution of the walls and therefore control of the microstructure. The factor of field type was considered in this analysis with five degrees of freedom, and a standard significance of $\alpha = 0.05$ was used.
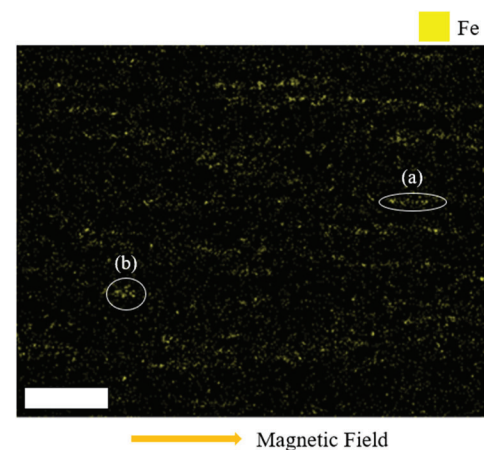

Fig. 4. EDS image detailing the distinction between a SPION-titania "wall" and "agglomeration". In (a) a wall is shown where there is a continuous string of particles at least 50 μm pointing in the same direction. In (b) an agglomeration is shown where there is no directionality of the particles, and they appear to form a cluster. The scale bar corresponds to 200 μm. (For interpretation of the references to color in this figure legend, the reader is referred to the web version of this article.).

3. Results and discussion

3.1. Helmholtz coils field validation

The percent error for the magnetic field magnitudes in the freeze cast workspace for both sets of coils can be seen in Table 1. Looking at all the percent errors, they are all very low, < 2 % error for both the large and small set of coils. These magnitudes of error are similar to previous research [34]. Therefore, it can be said with confidence that the bi-axial Helmholtz coils setup produces near uniform fields, as expected.

3.2. Surface magnetization results

The SPIONs on the surface of the titania microparticles can be distinctly identified in the TEM images (see Fig. 5a). Note that the SPIONS appear to be both attached and distributed across the surface of the titania microparticles, as opposed to not being attached to the microparticles. The magnetization curves for the surface-magnetized and non-surface-magnetized titania particles are shown in Fig. 5b. It was observed that the surface-magnetized titania had a much higher mass magnetization than the non-surface-magnetized titania. This is due to the SPIONs having a much higher magnetization compared to the titania microparticles. This increase in magnetization increases the ability of the particles to interact due to externally applied magnetic fields. The mass magnetization of titania changed by 2 emu/g at a 50 mT field strength, which is a large increase, but still significantly lower than the mass magnetization of iron oxide, which is a 40 emu/g change at a 50 mT field strength [34].

These results demonstrate that surface-magnetized particles can be achieved through the electrostatically interaction of SPIONs with the titania microparticles. The SPIONs were also shown to attach to the surface of the titania microparticles in an evenly distributed fashion. Therefore, due to the successful magnetization of surface-magnetized titania, it may be possible to successfully control these materials via magnetically assisted freeze casting.

3.3. Mechanical results

Fig. 6 shows the UCS as a function of the field type in the x- (UCS_x, applied-field direction) and y-direction (UCS_y, ice-growth direction). The 30 % Oscillation led to the strongest UCS_x, and the non-surface-magnetized scaffolds had the lowest UCS_x. All surface magnetized scaffolds had a higher UCS_x than the non-surface-magnetized scaffolds, with all p-values $\leq$ 2.90E-3. The 30 % Oscillation scaffolds had a strength an order of magnitude greater than the non-surface-magnetized scaffolds. The 30 % Oscillation was also significantly stronger than the No Field, with a p-value of 4.60E-2. In addition, although the Constant Field did not have a significant difference from the No Field or the 30 % Oscillation with an α = 0.05, the Constant Field and No Field were significantly different with 85 % confidence. A two-sample t-test was also run for the UCS_x to further validate the results between 30 % Oscillation and No Field surface-magnetized scaffolds. The t-test reported a p-value of 4.5E-2, thus further signifying increases in mechanical strength due to the application of the magnetic field type.

Looking at the UCS_y, all surface-magnetized scaffolds were stronger, and a statistically significant difference was observed compared to the non-surface-magnetized scaffolds with all p-values $\leq$ 1.6E-2. In addition, there was no statistically significant difference between the surface-magnetized scaffold field types, 30 % Oscillation, No Field, and Constant Field. Therefore, the strength of both the UCS_x and UCS_y was seen to increase through the application of the surface magnetization process, and the UCS_x was further increased by the application of the oscillating field.

The E_x and E_y were also analyzed for all field types, with no statistically significant differences observed. In a previous study, it was shown that applying an oscillating field led to a greater increase of strength in the x-direction when compared to when no field is applied [36]. This was explained by the oscillating fields theory, which was explained in a previous study [36], or that the application of the two fields simultaneously leads to more material response than when a single field is applied [36]. This agrees with the results, as it was shown the UCS_x significantly increased when the 30 % Oscillation was applied compared to No Field. Comparing these results to past magnetically assisted freeze casting of surface-magnetized titania, it can be seen that similar levels of increase of the mechanical strength in the applied field direction were achieved, however this was done at a much lower field strength (20 mT here vs. 120 mT in [39]) in addition to not weakening the strength in the ice-growth direction [39]. In addition, while error bars of a larger magnitude were reported, looking at previous freeze-casting research, comparable degrees of error can be seen in the mechanical data [38,45, 46], thus signifying that the degrees of error reported were not unusual or of a concern. Also, the One-way ANOVA test along with the two-sample t-test returned a significant value for the 30 % Oscillation to No Field for the surface magnetized scaffolds, thus signifying that the applied magnetic field type was most likely responsible for the increase in mechanical strength, as opposed to random effects. These results further cement the fact that applying oscillating fields to freeze-cast materials, including non-ferrimagnetic titania, led to strengthening of these structures in an additional direction to the ice-growth direction.

3.4. Microstructural results

To understand more fully why surface-magnetized scaffolds were significantly stronger than the non-surface-magnetized scaffolds, the microstructure was analyzed. Fig. 7 displays the average lamellar wall thickness and the percent porosity of each field type. The non-surface-magnetized scaffolds had the largest average wall thickness, being statistically significantly different compared to the other three field types, with all p-values < 1E-10. In contrast, it was also observed that the non-surface-magnetized scaffolds had the highest percent porosity, once again statistically significantly different from the other three field types, with all p-values $\leq$ 9.2E-6. These differences in porosity can be verified

Table 1

Percent error of workspace for the Helmholtz-coils setup. The data presented is the mean of ten measurements for two different field strengths at four locations, those being the center of the workspace (A), top center (B), top right (C), and center right (D). Percent error was calculated by subtracting the differences between the point in question to point A and dividing by Point A.

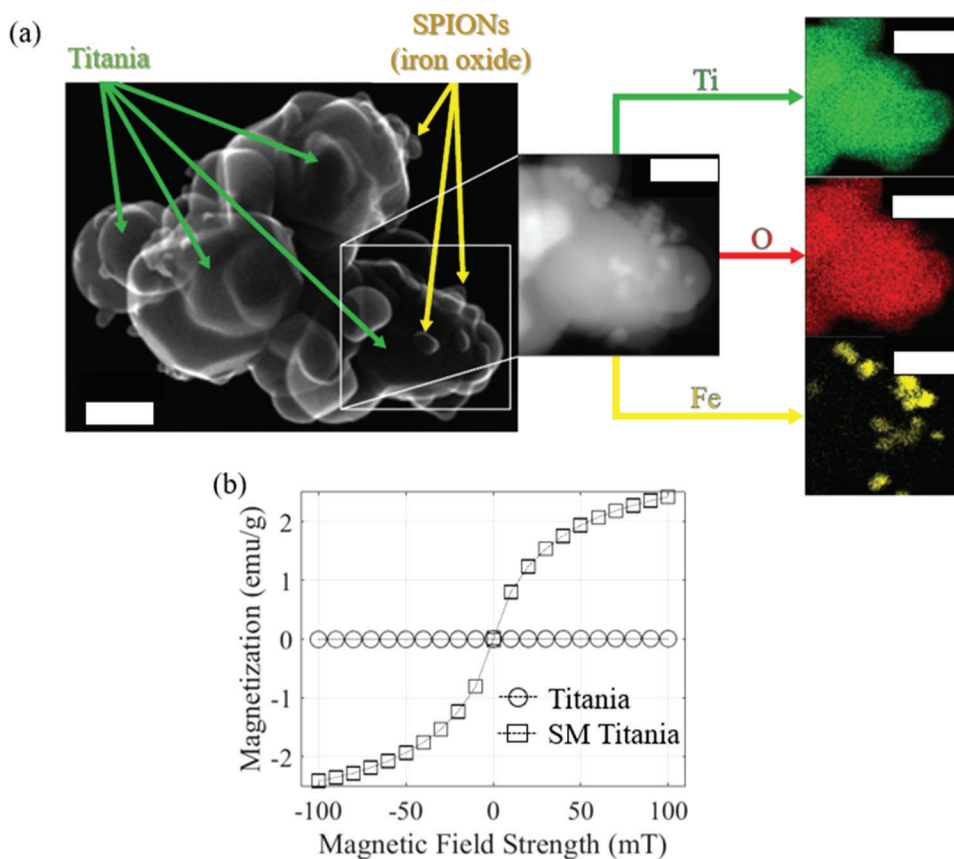| 5 mT – Large Coils		
Point	Magnitude (mT)	% error
A	5.01	0
B	4.98	0.53
C	5.00	0.10
D	4.97	0.63
5 mT – Small Coils		
Point	**Magnitude (mT)**	**% error**
A	5.09	0
B	5.01	1.6
C	5.14	1.0
D	5.10	0.03
7.5 mT – Small Coils		
Point	**Magnitude (mT)**	**% error**
A	7.71	0
B	7.62	1.1
C	7.84	1.7
D	7.69	0.28
7.5 mT – Large Coils		
Point	**Magnitude (mT)**	**% error**
A	7.35	0
B	7.33	1.2
C	7.36	0.20
D	7.36	0.08

Fig. 5. (a) TEM and EDS images of surface-magnetized particles made up of titania microparticles with SPIONs. (b) The magnetization curves for surface-magnetized and non-surface-magnetized titania. The scale bars correspond to 100 nm. (For interpretation of the references to color in this figure legend, the reader is referred to the web version of this article.).
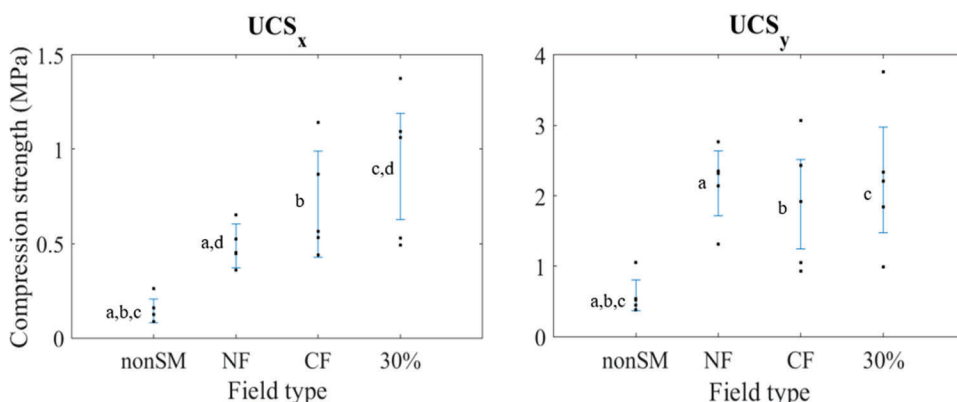

Fig. 6. Mean compression strength as a function of field type and surface magnetization, those being the non-surface-magnetized under 30 % Oscillation (nonSM), surface-magnetized scaffolds under No Field (NF), surface-magnetized scaffolds under Constant Field (CF), and surface-magnetized scaffolds under 30 % Oscillation (30 %). Data presented is the value from $n = 5$ scaffolds per field type, and the error bars represent the 95 % confidence interval on the mean. Comparisons that have statistically significant differences ($\alpha = 0.05$) are labeled by the same lower-case letter. (For interpretation of the references to color in this figure legend, the reader is referred to the web version of this article.).

by Fig. 8. Looking at the SEM image of a non-surface-magnetized scaffold in Fig. 8a, it appears to be much more porous than the surface-magnetized scaffold in Fig. 8b.

In addition to average porosity, Table 2 shows the average pore size and major and minor axis based on field type. The non-surface-magnetized scaffolds had the largest average pore area with 30 % Oscillation having the smallest, 30 % Oscillation had the largest average major axis with the non-surface-magnetized having the smallest, and the Constant Field had the largest minor axis with the non-surface-magnetized once again having the smallest. Therefore, even though the average lamellar wall is thicker in the non-surface-magnetized scaffolds, the much higher porosity and average pore size of these scaffolds led to larger pores in the structure, which would lead to weaker

structures when compared to more dense structures [14], as in the surface-magnetized scaffolds. One explanation for the denser microstructure in the surface-magnetized scaffolds is that the addition of the iron-oxide SPIONs, or ferrofluid, acted as a sintering aide, thus allowing the microstructure to fuse better than compared to the non-surface-magnetized scaffolds [47]. This is due to the lower temperature required to sinter or fuse the iron-oxide particles together compared to the titania particles (e.g. 1125 °C for iron oxide and 1200 °C for titania [18,34,36]). As the iron-oxide particles are attached to the titania particles, this causes the structure to densify sooner than if it were pure titania. It can therefore be concluded that the surface magnetization process strengthens freeze-cast structures when compared to non-surface-magnetized structures.
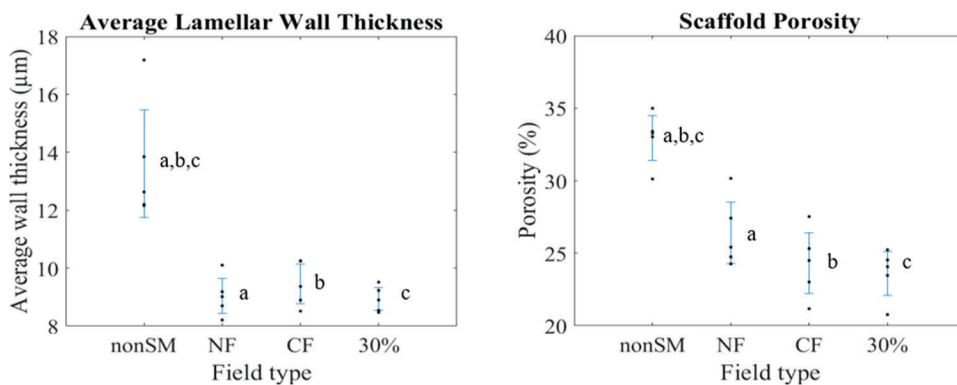
Fig. 7. Average lamellar wall thickness and scaffold porosity as a function of field type and surface magnetization, those being the non-surface-magnetized under 30 % Oscillation (nonSM), and surface-magnetized scaffolds under No Field (NF), surface-magnetized scaffolds under Constant Field (CF), and surface-magnetized scaffolds under 30 % Oscillation (30 %). Data presented is the values from $n = 5$ scaffolds per field type, and the error bars represent the 95 % confidence interval on the mean. Comparisons that have statistically significant differences ($\alpha = 0.05$) are labeled by the same lower-case letter. (For interpretation of the references to color in this figure legend, the reader is referred to the web version of this article.).
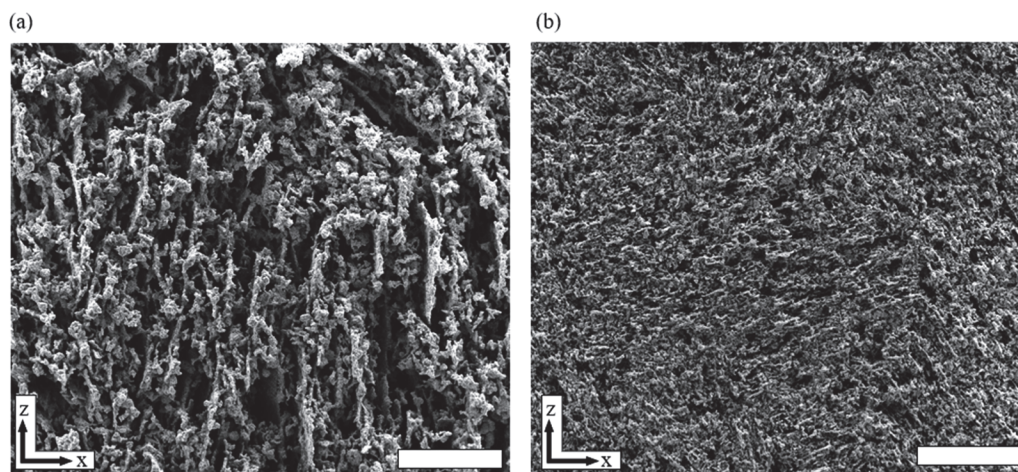

Fig. 8. SEM images visualizing the differences in average porosity between a non-surface magnetized freeze-cast scaffold (a), and a surface magnetized freeze-cast scaffold fabricated under the 30 % Oscillation (b). The scale bars correspond to 250 μm. (For interpretation of the references to color in this figure legend, the reader is referred to the web version of this article.).

Table 2
The microstructural properties as a function of all field types, including the average pore area, average major axis, and average minor axis. All data is reported as the mean ± one standard deviation of 4400 measurements for $n = 5$ scaffolds for each field type. Comparisons that have statistically significant differences ($\alpha = 0.05$) are labeled by the same lower-case letter.

Magnetic field type	Pore area (μm²)	Major axis (μm)	Minor axis (μm)
Non-surface Magnetized	185 ± 63.9(a,b)	14.2 ± 2.66(a)	6.61 ± 1.02(a,b)
No field	140 ± 15.7	14.9 ± 1.03(a)	7.34 ± 0.53(a)
Constant field	128 ± 35.1(a)	15.4 ± 1.47	7.57 ± 0.83(b)
30 % Oscillation	120 ± 23.3(b)	16.5 ± 0.86	7.54 ± 0.37

In addition to surface-magnetized scaffolds being stronger than non-surface-magnetized scaffolds, it was shown that the 30 % Oscillation scaffolds were the strongest overall. Further investigation can be done with the microstructure to explain the cause. This analysis was done by first analyzing the alignment of the lamellar walls on the x-z face. After analyzing the wall alignment, no directionality or control over the lamellar walls was seen by any field type (see Sup Fig. 1). Next, the directionality of the SPION-titania walls was analyzed for each field type, as can be seen in Fig. 9. Starting with the No Field, it can be seen in Fig. 9a that very few walls aligned in the x-direction. This can be seen by looking at the EDS image of the No Field in Fig. 9d, where very few walls seem to be aligned in the x-direction. This was verified with a chi-squared value of $\chi^2 = 10.1$ which corresponds to $p > 0.05$, and

therefore it can be concluded that there was an approximately even dispersion of walls in every sector, and differences in the SPION-titania wall alignment can be explained by random effects. For the Constant Field, it can be seen in Fig. 9b that there was more control and alignment of the walls in the x-direction, that being the 0° sector. This can be seen in Fig. 9e, where the highest percent of walls aligned in the applied field direction. This was also verified with a chi-squared value of $\chi^2 = 14.2$ which corresponds to $p < 2.5E-2$, signifying that differences observed cannot be explained by random chance. The 0° sector was favored, with the highest percent of walls, and therefore a degree of control over the SPION-titania walls was achieved in the x-direction. The 30 % Oscillation further increased this control and alignment, as can be seen in Fig. 9c, with an even larger percentage of the walls aligned in the 0° sector. This further control of the microstructure can be seen in Fig. 9f, where walls tended to align in the x-direction. This was also verified with a chi-squared value of $\chi^2 = 34.2$ which corresponds to $p < 5E-3$. The 0° sector was therefore favored, with the highest percent of walls, and the greatest amount of control over the SPION-titania walls achieved in the x-direction.

These aligned SPION-titania walls led to mineral bridges in between the lamellar walls, which is hypothesized to be what led to the further strengthening of the 30 % Oscillation scaffolds (see Fig. 10). These mineral bridges have been produced in previous magnetically assisted freeze casting, where additional mechanical strength was also observed [31]. The distribution of the SPIONs as seen in Fig. 9d-f is likely due to how the SPIONs were attached evenly across the outside surface of the titania microparticles (as seen in Fig. 5a). These "gaps" seen in the EDS
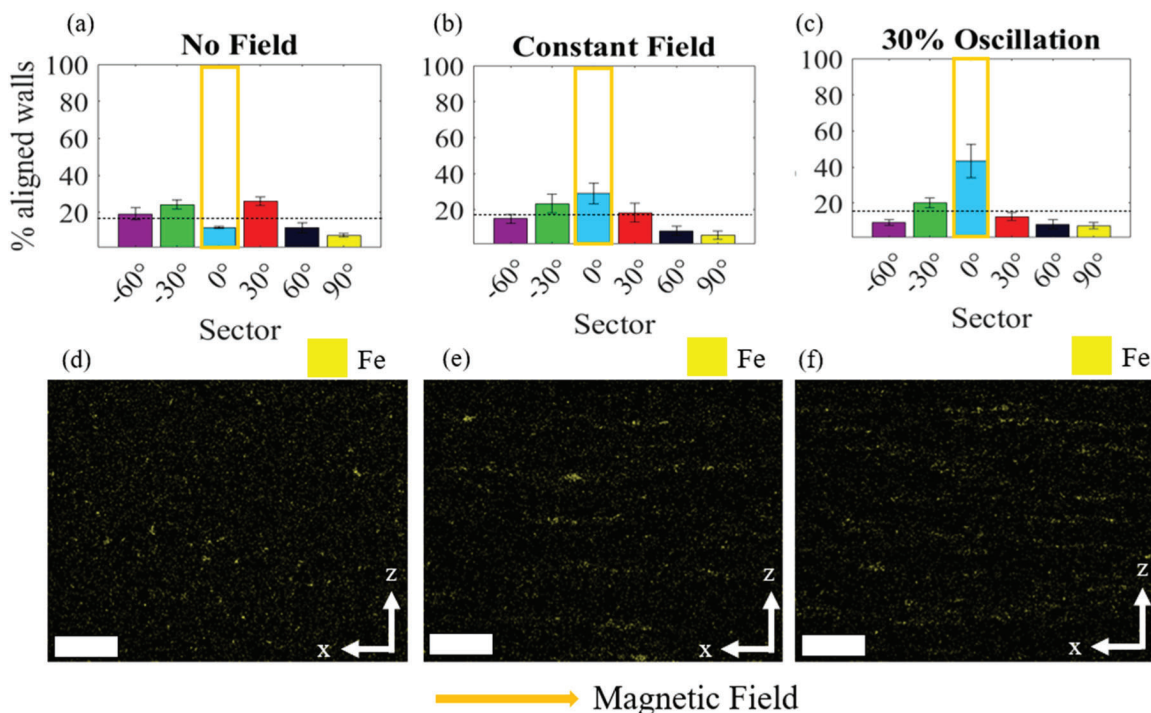
Fig. 9. (a-c) Percent of SPION-titania walls that align in each sector for each field type with surface-magnetized scaffolds. The direction of the applied field is in the 0° sector. Data presented is the mean value obtained from $n = 3$ scaffolds per field type, and the error bars represent ±one standard deviation. The dotted line indicates the expected value due to random chance. The chi-square goodness of fit analysis with $\alpha = 0.05$ determined that differences in the distribution of the SPION-titania walls for the No Field case could be explained by random chance, whereas for the Constant Field and 30 % Oscillation a significantly unequal distribution of the SPION-titania walls was observed, with the largest proportion in the 0° sector, and therefore control of the walls was observed for these two field types. (d-f) EDS image of the SPIONs for each surface magnetized field type from left to right: No Field, Constant Field, 30 % Oscillation. The direction of the applied field is in the x-direction. All scale bars correspond to 200 μm. (For interpretation of the references to color in this figure legend, the reader is referred to the web version of this article.).
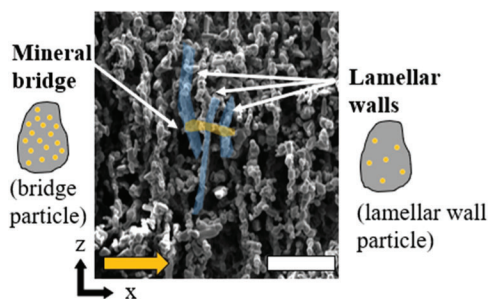

Fig. 10. SEM image showing the mineral bridges that form as a magnetic field is applied due to the alignment of the SPION-titania walls as well as a visualization of how more SPIONs (pictured as orange dots) tend to be attached to the titania particles in the mineral bridges then compared to the lamellar walls. The orange bar is the field direction. The scale bar corresponds to 50 μm. (For interpretation of the references to color in this figure legend, the reader is referred to the web version of this article.).

images can be likened as the center of the titania microparticles, with the SPIONs along the surface being the catalyst that forms the bridges between the lamellar walls. In addition, the lack of alignment of the lamellar walls as opposed to the alignment of the SPION-titania bridges can be attributed to the uneven distribution of the SPIONs across the microstructure. It has been shown in previous research that the bridges had a higher concentration of SPIONs when compared to the lamellar walls (upwards of 3 %) [38]. The bridges were therefore comprised of the titania particles with a higher concentration of SPIONs when compared to the lamellar walls, which had a lower concentration of SPIONs (see Fig. 10 for a visual representation), which led to greater control over the bridges compared to the lamellar walls.

These results show that, through the use of the surface-magnetization process, the microstructure of freeze-cast structures can be controlled and strengthened when compared to non-surface-magnetized structures. In addition, it was shown that the application of oscillating fields during the freeze-casting process further increases microstructural control and strengthens the structure. Therefore, even though the mass magnetization of surface-magnetized titania was significantly lower than iron oxide, through the use of oscillating fields, surface-magnetized titania can still be successfully controlled during the freeze-casting process. When comparing to other methods of controlling alignment of titania freeze-cast structures, for example the application of ultrasound waves during the freeze-cast process [48], it can be seen that although similar control over porosity and alignment is achieved, no increase in mechanical strength was observed [48]. Therefore, it can be stated that, through the application of both the surface magnetization process and the application of oscillating fields, not only can this microstructural control be achieved similar to previous control methods, but the mechanical properties of the structure can be strengthened as well.

4. Conclusions

Based on this study of applying a surface-magnetized process to titania, and the application of oscillating magnetic fields produced a bi-axial Helmholtz coils setup to titania freeze-cast structures, the following conclusions can be drawn:

1 Through the use of the surface-magnetization process, non-ferrimagnetic titania can be successfully surface magnetized, resulting in an increase in the mass magnetization.

2 The mechanical properties of titania freeze-cast structures can be strengthened through the use of the surface-magnetization process. An increase of 10x in UCS_x, the applied magnetic field direction, was observed when comparing the 30 % Oscillation surface-magnetized scaffolds to the non-surface-magnetized scaffolds.

3 The mechanical properties of surface-magnetized titania freeze-cast structures can be further strengthened through the application of oscillating fields during the freeze-casting process. An increase of 2x in UCS_x was seen when applying the 30 % Oscillation compared to No Field.

4 The microstructure of surface-magnetized titania freeze-cast structures can be controlled through the application of oscillating fields as well. It was seen that the SPION-titania bridges tended to align in the applied field direction when the 30 % Oscillation was applied.

5 Applying an oscillating field to surface-magnetized titania freeze-cast structures can lead to control over the microstructure and an associate increase in UCS in the x-direction.

Declaration of Competing Interest

The authors declare that they have no known competing financial interests or personal relationships that could have appeared to influence the work reported in this paper.

Acknowledgements

Supplementary materials

Supplementary material associated with this article can be found, in the online version, at doi:10.1016/j.mtla.2023.101905.

References

[1] S.W. Sofie, F. Dogan, Freeze casting of aqueous alumina slurries with glycerol, J. Am. Ceram. Soc. 84 (7) (2001) 7, https://doi.org/10.1111/j.1151-2916.2001.tb00860.x. Art. no.

[2] K. Araki, J.W. Halloran, Porous ceramic bodies with interconnected pore channels by a novel freeze casting technique, J. Am. Ceram. Soc. 88 (5) (2005) 5, https://doi.org/10.1111/j.1551-2916.2005.00176.x. Art. no.

[3] H.-W. Kang, Y. Tabata, Y. Ikada, Fabrication of porous gelatin scaffolds for tissue engineering, Biomaterials 20 (14) (Jul. 1999) 14, https://doi.org/10.1016/S0142-9612(99)00036-8. Art. no.

[4] H. Schoof, J. Apel, I. Heschel, G. Rau, Control of pore structure and size in freeze-dried collagen sponges, J. Biomed. Mater. Res. 58 (4) (2001), 4, https://doi.org/10.1002/jbm.1028. Art. no.

[5] M.V. Dinu, M. Přádný, E.S. Drăgan, J. Michálek, Ice-templated hydrogels based on chitosan with tailored porous morphology, Carbohydr. Polym. 94 (1) (Apr. 2013), 1, https://doi.org/10.1016/j.carbpol.2013.01.084. Art. no.

[6] N.L. Francis, et al., An ice-templated, linearly aligned chitosan-alginate scaffold for neural tissue engineering, J. Biomed. Mater. Res. A 101 (12) (2013), 12, https://doi.org/10.1002/jbm.a.34668. Art. no.

[7] T. Köhnke, T. Elder, H. Theliander, A.J. Ragauskas, Ice templated and cross-linked xylan/nanocrystalline cellulose hydrogels, Carbohydr. Polym. 100 (Jan. 2014) 24–30, https://doi.org/10.1016/j.carbpol.2013.03.060.

[8] H.-D. Jung, S.-W. Yook, H.-E. Kim, Y.-H. Koh, Fabrication of titanium scaffolds with porosity and pore size gradients by sequential freeze casting, Mater. Lett. 63 (17) (Jul. 2009), 17, https://doi.org/10.1016/j.matlet.2009.04.012. Art. no.

[9] H.-D. Jung, S.-W. Yook, T.-S. Jang, Y. Li, H.-E. Kim, Y.-H. Koh, Dynamic freeze casting for the production of porous titanium (Ti) scaffolds, Mater. Sci. Eng. C 33 (1) (Jan. 2013), 1, https://doi.org/10.1016/j.msec.2012.08.004. Art. no.

[10] Y. Chino, D.C. Dunand, Directionally freeze-cast titanium foam with aligned, elongated pores, Acta Mater. 56 (1) (Jan. 2008), 1, https://doi.org/10.1016/j.actamat.2007.09.002. Art. no.

[11] J.C. Li, D.C. Dunand, Mechanical properties of directionally freeze-cast titanium foams, Acta Mater. 59 (1) (Jan. 2011), 1, https://doi.org/10.1016/j.actamat.2010.09.019. Art. no.

[12] S.E. Naleway, et al., Bioinspired composites from freeze casting with clathrate hydrates, Mater. Des. 71 (Apr. 2015) 62–67, https://doi.org/10.1016/j.matdes.2015.01.010.

[13] S. Roy, A. Wanner, Metal/ceramic composites from freeze-cast ceramic preforms: domain structure and elastic properties, Compos. Sci. Technol. 68 (5) (Apr. 2008), 5, https://doi.org/10.1016/j.compscitech.2007.06.013. Art. no.

[14] S. Deville, Freeze-casting of porous ceramics: a review of current achievements and issues, Adv. Eng. Mater. 10 (3) (2008), 3, https://doi.org/10.1002/adem.200700270. Art. no.

[15] S. Deville, E. Saiz, A.P. Tomsia, Ice-templated porous alumina structures, Acta Mater 55 (6) (Apr. 2007), 6, https://doi.org/10.1016/j.actamat.2006.11.003. Art. no.

[16] E. Munch, J. Franco, S. Deville, P. Hunger, E. Saiz, A.P. Tomsia, Porous ceramic scaffolds with complex architectures, JOM 60 (6) (Jun. 2008), 6, https://doi.org/10.1007/s11837-008-0072-5. Art. no.

[17] T.A. Ogden, Bioinspired Ultrasound Freeze Casting: Engineered Porous Scaffolds Through Freeze Casting and Ultrasound Directed Self-Assembly, The University of Utah, United States – Utah, 2019. M.S.Accessed: Aug. 25, 2021. [Online]. Available, https://www.proquest.com/docview/2496206030/abstract/4F4366FD0D0E4001PQ/1.

[18] I. Nelson, L. Gardner, K. Carlson, S.E. Naleway, Freeze casting of iron oxide subject to a tri-axial nested Helmholtz-coils driven uniform magnetic field for tailored porous scaffolds, Acta Mater. 173 (Jul. 2019) 106–116, https://doi.org/10.1016/j.actamat.2019.05.003.

[19] M.B. Frank, et al., Synergistic structures from magnetic freeze casting with surface magnetized alumina particles and platelets, J. Mech. Behav. Biomed. Mater. 76 (Dec. 2017) 153–163, https://doi.org/10.1016/j.jmbbm.2017.06.002.

[20] S.E. Naleway, K.C. Fickas, Y.N. Maker, M.A. Meyers, J. McKittrick, Reproducibility of ZrO2-based freeze casting for biomaterials, Mater. Sci. Eng. C 61 (Apr. 2016) 105–112, https://doi.org/10.1016/j.msec.2015.12.012.

[21] S. Deville, et al., In situ x-ray radiography and tomography observations of the solidification of aqueous alumina particle suspensions—Part I: initial instants, J. Am. Ceram. Soc. 92 (11) (2009), 11, https://doi.org/10.1111/j.1551-2916.2009.03163.x. Art. no.

[22] S. Deville, et al., Metastable and unstable cellular solidification of colloidal suspensions, Nat. Mater. 8 (12) (Dec. 2009) 966–972, https://doi.org/10.1038/nmat2571.

[23] P.M. Hunger, A.E. Donius, U.G.K. Wegst, Structure–property-processing correlations in freeze-cast composite scaffolds, Acta Biomater. 9 (5) (May 2013), 5, https://doi.org/10.1016/j.actbio.2013.01.012. Art. no.

[24] S.W. Sofie, Fabrication of functionally graded and aligned porosity in thin ceramic substrates with the novel freeze–tape-casting process, J. Am. Ceram. Soc. 90 (7) (2007), 7, https://doi.org/10.1111/j.1551-2916.2007.01720.x. Art. no.

[25] L. Qian, H. Zhang, Controlled freezing and freeze drying: a versatile route for porous and micro-/nano-structured materials, J. Chem. Technol. Biotechnol. 86 (2) (2011), 2, https://doi.org/10.1002/jctb.2495. Art. no.

[26] P.M. Hunger, A.E. Donius, U.G.K. Wegst, Platelets self-assemble into porous nacre during freeze casting, J. Mech. Behav. Biomed. Mater. 19 (Mar. 2013) 87–93, https://doi.org/10.1016/j.jmbbm.2012.10.013.

[27] A. Preiss, B. Su, S. Collins, D. Simpson, Tailored graded pore structure in zirconia toughened alumina ceramics using double-side cooling freeze casting, J. Eur. Ceram. Soc. 32 (8) (Jul. 2012), 8, https://doi.org/10.1016/j.jeurceramsoc.2011.12.031. Art. no.

[28] H. Bai, Y. Chen, B. Delattre, A.P. Tomsia, R.O. Ritchie, Bioinspired large-scale aligned porous materials assembled with dual temperature gradients, Sci. Adv. 1 (11) (Dec. 2015), 11, https://doi.org/10.1126/sciadv.1500849. Art. no.

[29] H. Bai, et al., Bioinspired hydroxyapatite/Poly(methyl methacrylate) composite with a Nacre-Mimetic architecture by a bidirectional freezing method, Adv. Mater. 28 (1) (2016), 1, https://doi.org/10.1002/adma.201504313. Art. no.

[30] H. Bai, et al., Biomimetic gradient scaffold from ice-templating for self-seeding of cells with capillary effect, Acta Biomater. 20 (Jul. 2015) 113–119, https://doi.org/10.1016/j.actbio.2015.04.007.

[31] J.-W. Moon, H.-J. Hwang, M. Awano, K. Maeda, Preparation of NiO–YSZ tubular support with radially aligned pore channels, Mater. Lett. 57 (8) (Feb. 2003), 8, https://doi.org/10.1016/S0167-577X(02)01002-9. Art. no.

[32] Y. Tang, Q. Miao, S. Qiu, K. Zhao, L. Hu, Novel freeze-casting fabrication of aligned lamellar porous alumina with a centrosymmetric structure, J. Eur. Ceram. Soc. 34 (15) (Dec. 2014), 15, https://doi.org/10.1016/j.jeurceramsoc.2014.05.040. Art. no.

[33] Y. Tang, S. Qiu, Q. Miao, C. Wu, Fabrication of lamellar porous alumina with axisymmetric structure by directional solidification with applied electric and magnetic fields, J. Eur. Ceram. Soc. 36 (5) (Apr. 2016), 5, https://doi.org/10.1016/j.jeurceramsoc.2015.12.012. Art. no.

[34] I. Nelson, et al., Freeze-casting of surface-magnetized iron(II,III) oxide particles in a uniform static magnetic field generated by a helmholtz coil, Adv. Eng. Mater. 21 (3) (2019), 3, https://doi.org/10.1002/adem.201801092. Art. no.

[35] M.B. Frank, et al., Stiff, porous scaffolds from magnetized alumina particles aligned by magnetic freeze casting, Mater. Sci. Eng. C 77 (Aug. 2017) 484–492, https://doi.org/10.1016/j.msec.2017.03.246.

[36] J.R. Fernquist, H.C. Fu, S.E. Naleway, Improved structural and mechanical performance of iron oxide scaffolds freeze cast under oscillating magnetic fields, Ceram. Int. 48 (11) (Jun. 2022), 11, https://doi.org/10.1016/j.ceramint.2022.02.032. Art. no.

[37] I. Nelson, S.E. Naleway, Intrinsic and extrinsic control of freeze casting, J. Mater. Res. Technol. 8 (2) (Apr. 2019), 2, https://doi.org/10.1016/j.jmrt.2018.11.011. Art. no.

[38] M.M. Porter, P. Niksiar, J. McKittrick, Microstructural control of colloidal-based ceramics by directional solidification under weak magnetic fields, J. Am. Ceram. Soc. 99 (6) (2016), 6, https://doi.org/10.1111/jace.14183. Art. no.

[39] M.M. Porter, et al., Magnetic freeze casting inspired by nature, Mater. Sci. Eng. A 556 (Oct. 2012) 741–750, https://doi.org/10.1016/j.msea.2012.07.058.

[40] J.J. Abbott, Parametric design of tri-axial nested Helmholtz coils, Rev. Sci. Instrum. 86 (5) (May 2015), 5, https://doi.org/10.1063/1.4919400. Art. no.

[41] I. Nelson, et al., Helical and bouligand porous scaffolds fabricated by dynamic low strength magnetic field freeze casting, JOM 72 (4) (Apr. 2020), 4, https://doi.org/10.1007/s11837-019-04002-9. Art. no.

[42] T.J. Yin, S. Jeyapalina, S.E. Naleway, Characterization of porous fluorohydroxyapatite bone-scaffolds fabricated using freeze casting, J. Mech. Behav. Biomed. Mater. 123 (Nov. 2021), 104717, https://doi.org/10.1016/j.jmbbm.2021.104717.

[43] D. Shi, et al., Magnetic alignment of Ni/Co-coated carbon nanotubes in polystyrene composites, Compos. PART B-Eng. 42 (6) (Sep. 2011) 1532–1538, https://doi.org/10.1016/j.compositesb.2011.04.014.

[44] J. Ma and K. Chen, "Surface-modulated magnetization of magnetite microspheres," *Phys. Status Solidi RRL – Rapid Res. Lett.*, vol. 6, no. 9–10, pp. 391–393, 2012, doi: 10.1002/pssr.201206292.

[45] A.M.A. Silva, et al., Effect of titania addition on the properties of freeze-cast alumina samples, Ceram. Int. 41 (9) (Nov. 2015), 9, https://doi.org/10.1016/j.ceramint.2015.04.132. Part A, Art. noPart A.

[46] N. Nezafati, M. Hafezi, A. Zamanian, M. Naserirad, Effect of adding nano-titanium dioxide on the microstructure, mechanical properties and in vitro bioactivity of a freeze cast merwinite scaffold, Biotechnol. Prog. 31 (2) (2015) 550–556, https://doi.org/10.1002/btpr.2042.

[47] T.S. Zhang, J. Ma, L.B. Kong, S.H. Chan, P. Hing, J.A. Kilner, Iron oxide as an effective sintering aid and a grain boundary scavenger for ceria-based electrolytes, Solid State Ion 167 (1) (Feb. 2004) 203–207, https://doi.org/10.1016/j.ssi.2004.01.006.

[48] T.A. Ogden, M. Prisbrey, I. Nelson, B. Raeymaekers, S.E. Naleway, Ultrasound freeze casting: fabricating bioinspired porous scaffolds through combining freeze casting and ultrasound directed self-assembly, Mater. Des. 164 (Feb. 2019), 107561, https://doi.org/10.1016/j.matdes.2018.107561.